SCIENCE CHINA
Physics, Mechanics & Astronomy

•Article•

June 2020 Vol. 63 No. 6: 267811
https://doi.org/10.1007/s11433-019-1494-4

Single-electron pumping in a ZnO single-nanobelt quantum dot transistor

Hassan Ali[1,6], Jing Tang[1,2], Kai Peng[1], SiBai Sun[1], Attia Falak[3,4], FeiLong Song[1], ShiYao Wu[1], ChenJiang Qian[1], Meng Wang[1], XiTian Zhang[5], Muhammad Aftab Rafiq[6], and XiuLai Xu[1,7,8*]

[1] *Beijing National Laboratory for Condensed Matter Physics, Institute of Physics, Chinese Academy of Sciences, Beijing 100190, China;*
[2] *Laboratory of Quantum Engineering and Quantum Metrology, School of Physics and Astronomy, Sun Yat-Sen University (Zhuhai Campus), Zhuhai 519082, China;*
[3] *National Center for Nanoscience and Technology, Chinese Academy of Sciences, Beijing 100190, China;*
[4] *Department of Physics, University of the Punjab, Quaid-e-Azam Campus, Lahore 54000, Pakistan;*
[5] *Key Laboratory for Photonic and Electronic Bandgap Materials, Ministry of Education, School of Physics and Electronic Engineering, Harbin Normal University, Harbin 150025, China;*
[6] *Department of Physics and Applied Mathematics, Pakistan Institute of Engineering and Applied Sciences, Islambad 45650, Pakistan;*
[7] *CAS Center for Excellence in Topological Quantum Computation, School of Physical Sciences, University of Chinese Academy of Sciences, Beijing 100190, China;*
[8] *Songshan Lake Materials Laboratory, Dongguan 523808, China;*

Received November 7, 2019; accepted December 10, 2019; published online February 18, 2020

Diluted magnetic semiconductors (DMSs) have traditionally been employed to implement spin-based quantum computing and quantum information processing. However, their low Curie temperature is a major hurdle in their use in this field, which creates the necessity for wide bandgap DMSs operating at room temperature. In view of this, a single-electron transistor (SET) with a global back-gate was built using a wide bandgap ZnO nanobelt (NB). Clear Coulomb oscillations were observed at 4.2 K. The periodicity of the Coulomb diamonds indicates that the Coulomb oscillations arise from single quantum dots of uniform size, whereas quasi-periodic Coulomb diamonds correspond to the contribution of multi-dots present in the ZnO NB. By applying an AC signal to the global back-gate across a Coulomb peak with varying frequencies, single-electron pumping was observed; the increase in current was equal to the production of electron charge and frequency. The current accuracy of about 1% for both single- and double-electron pumping was achieved at a high frequency of 25 MHz. This accurate single-electron pumping makes the ZnO NB SET suitable for single-spin injection and detection, which has great potential for applications in quantum information technology.

ZnO nanobelt, Coulomb blockade, quantum dot transistor, single-electron pumping

PACS number(s): 68.65.La, 72.80.Ey, 72.23.Hk, 73.21.Hb

Citation: H. Ali, J. Tang, K. Peng, S. B. Sun, A. Falak, F. L. Song, S. Y. Wu, C. J. Qian, M. Wang, X. T. Zhang, M. A. Rafiq, and X. L. Xu, Single-electron pumping in a ZnO single-nanobelt quantum dot transistor, Sci. China-Phys. Mech. Astron. **63**, 267811 (2020), https://doi.org/10.1007/s11433-019-1494-4

*Corresponding author (email: xlxu@iphy.ac.cn)

1 Introduction

Spintronics has emerged as a tool to utilize electronic spin as a new parameter for data storage and quantum information processing with low power consumption. In spintronics, electron spin and orbital momentum are crucial parameters and can enhance the functionality of electronic devices. In order to control the properties of semiconductor quantum structure along with magnetic phenomenon in terms of spin, current, and carrier populations, multifunctional materials such as diluted magnetic semiconductors (DMSs) emerged [1,2]. In DMSs, it was found that the magnetic properties in host materials could be formed by introducing small portions of magnetic materials and that their optoelectronic transport properties did not concurrently degrade [2]. This has led to DMSs attracting enormous attention for their huge potential in the applications of spintronics. Many DMSs, such as indium-doped Mn_5Ge_3 and (Ga, Mn)As, have been used for precise spin injection and detection purposes [3,4]. However, their low Curie temperatures, caused by narrow bandgap, limit application at room temperature. Therefore, wide bandgap semiconductor materials such as ZnO doped with transition metals are highly desirable [2].

ZnO has been employed in numerous applications such as solar cells, light-emitting diodes, field-effect transistors, nanolasers, gas sensors, photodetectors, spintronic devices, and piezo-electronic nanogenerators [5-13]. ZnO's wide bandgap also makes it a prospective candidate for room temperature spintronic devices [14]. Furthermore, the properties of ZnO can be improved by introducing different dopants: for example, the doping of transition metals in ZnO can improve its ferromagnetic properties, which are advantageous for future applications in spintronics [15,16]. Among these ZnO materials, ZnO nanobelts (NBs) are attractive candidates for optoelectronic and nanoscale electronic applications because of the direct wide bandgap (3.37 eV), high exciton binding energy at room temperature (60 meV), and large surface-to-volume ratio.

Being highly charge sensitive, single-electron transistors (SETs) are ideal for studying quantum effects such as Coulomb blockade, tunneling, and single-electron pumping [17-22] and have shown vast applications in charge detection, thermometry, single-spin detection, single-photon detection, and detection of nano-electro-mechanical motion [20-28]. Other types of single-electron device (quantized charge pump) have also gained tremendous significance because of their numerous applications in metrology, single-spin initialization, single-electron logic circuits, deterministic single-photon sources, and solid-state quantum computing technology [29-36].

To date, single-electron tunneling-based devices such as SETs and single-electron pumps have been investigated using metal [30,37], Au nanoparticles [18,38], carbon nanotubes [29], graphene [34], and semiconducting materials such as Si [22,39-41], GaAs [42-44], and InP and InP/InAs heterostructures [25,45,46]. Indium arsenide phosphide quantum dots [47] and DMSs (Ga, Mn)As-based SETs [48] have also been employed for spin storage and single-electron charging. To the best of our knowledge, only a few studies on ZnO NB SETs [5,6] have been conducted, and there has been no research into the advantages for single-electron spin control of single-electron pumping in ZnO quantum dots.

In this work, SETs based on single indium-doped ZnO NB were built. The doping concentration of indium in ZnO was 1.1 percent. Clear Coulomb oscillations in the SETs were observed at 4.2 K. The contributions from the single localized quantum dots and multi-dots to the output current were observed for different applied gate bias regimes. Single- and double-electron pumping was also achieved by using a back-gated AC signal for different pumping voltages. The realization of controlled single- and double-electron pumping in ZnO quantum dots with the simplest configuration was a significant step toward understanding the coherent properties of electron spin in quantum dots for future applications. These results indicate that ZnO NBs are promising candidates for single-electron spin detection, which is useful for quantum computing and quantum information. Furthermore, the simple configuration of the device used in our work will make it more compatible with standard Si technology in the future.

2 Experimental details

The indium-doped ZnO NBs were grown by the chemical vapor deposition technique; details of the growth process have been reported elsewhere [49,50]. Morphological information on the NBs was obtained using scanning electron microscopy. The average length of NBs was 5 μm with a width of up to 300 nm. A back-gated SET was designed on the basis of these indium-doped ZnO NBs. The as-grown NBs were dispersed in isopropyl alcohol and sonicated to form a homogeneous solution of nanowires before being spin-coated on Si substrate (patterned by standard ultraviolet lithography) coated with SiO_2 with a thickness of 300 nm. The location of NBs on the substrate was traced by scanning electron microscopy. The patterns for source and drain electrodes on individual NBs were then designed by standard electron beam lithography, followed by metal deposition (20 nm/70 nm, Cr/Au) and lift-off in acetone. Si substrate was used as a back-gate for SETs. The electrical characterizations were performed by semiconductor parameter analyzer with a current resolution of up to 1 fA at room and low temperatures of 4.2 K. The low-temperature measurements were performed in a liquid helium dewar.

3 Results and discussion

In general, an SET consists of a conducting island (quantum dot) coupled to two metal electrodes, namely, the source and drain, via tunnel junctions. The island is capacitively coupled to a third metal electrode called a gate [18,20,51]. The quantum dots that act as artificial atoms provide three dimensional confinement in which the motion of the electrons is confined to a nanometer-sized region. The energy levels of electrons in quantum dots are quantized as in the case of atoms [52]. The minimum energy required to add an electron on the island is known as charging energy, which is much larger than the thermal energy of electrons [23,46,52,53]. Under this condition, the "charging effect" emerges because of the discreteness of electron tunneling [30]. The single-electron charging of the island can be controlled by back-gate bias [24,46,54].

The schematic diagram and scanning electron micrograph of the ZnO single NB SET are shown in Figure 1(a) and (b), respectively; channel length and width are ~5 μm and ~400 nm, respectively. The output characteristics (source-drain current I_{ds} as a function of source-drain voltage V_{ds}) of the ZnO NB SET at room temperature for different gate voltages (V_g) are shown in Figure 1(c). It should be noted that I_{ds} increases linearly with V_{ds} at all V_g, indicating good Ohmic contact between the ZnO NB and metal electrodes. Furthermore, I_{ds} increasing with V_g reveals the n-type nature of the ZnO NB. Linear dependence of I_{ds} on V_g implies that modulation in carrier density in the ZnO NB can be achieved by V_g. The transfer characteristics (I_{ds}-V_g) of the ZnO NB SET at room temperature are shown in Figure 1(d). The I_{ds} increases as V_g increases at constant V_{ds}, which also confirms the n-type nature of the ZnO NB.

The I_{ds}-V_{ds} characteristics of the ZnO NB SET at 4.2 K are shown in Figure 2(a). Here I_{ds} does not depend linearly on V_{ds}, and the slopes of the I_{ds}-V_{ds} curves are different in different V_{ds} regimes. The slope is almost flat for low values of V_{ds} and then becomes positive for high V_{ds} values. The I_{ds}-V_g curves with V_{ds} from −20 to 20 mV are shown in Figure 2(b). The I_{ds} does not increase linearly with V_g. However, oscillating behavior of I_{ds} with V_g is observed with different V_{ds}. The oscillating amplitude increases with the increase in V_{ds} and decreases at lower V_{ds} [5,6]. The fluctuation in V_g means that the blockade of current tunneling through the barrier varies from zero to non-zero values, which in turn manifests the oscillating behavior of the current. This oscillating behavior with gate voltage results in the emergence of current oscillations known as Coulomb oscillations. This blockade effect can be exploited by transferring the charges in a controlled way from one island to the other or from island to drain electrode [6,23,37,46,52,54].

To strengthen the claim of observed Coulomb oscillations in the transfer characteristics of the ZnO NB SET, the differential trans-conductance (g_m=dI_{ds}/dV_g) versus V_g is plotted in Figure 3(a) and (b) at 4.2 K. Clear Coulomb oscillations are observed in Figure 3(a) and (b). The period of oscillations in Figure 3(a) is the same, signifying that only a single quantum dot is contributing to the change in current [5,24,46]. However, in the case of Figure 3(b), the period of oscillations is different for different V_g regimes, which can be attributed to the contribution from more than one quantum dots in ZnO NB nanobelt; this can be explained by the

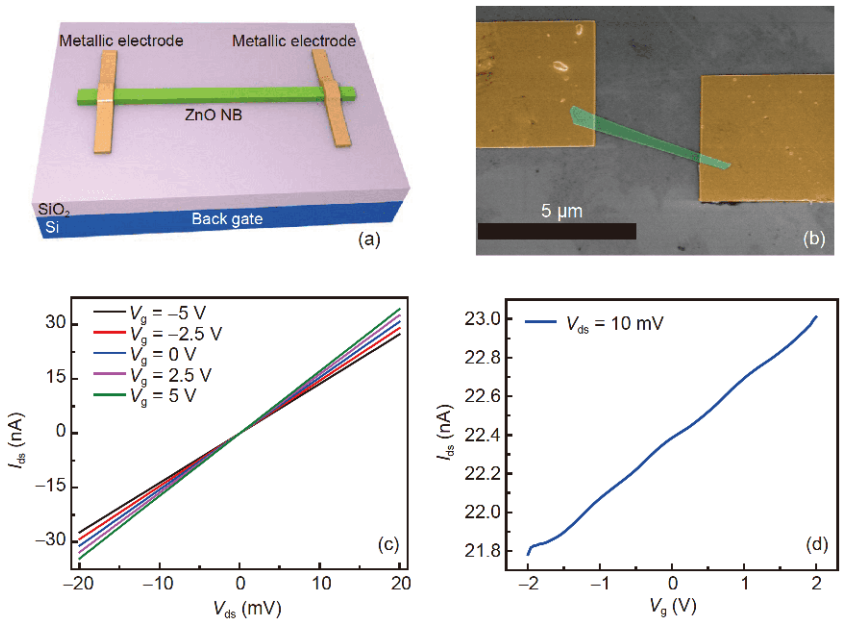

Figure 1 (Color online) (a) Schematic diagram and (b) scanning electron micrograph of the ZnO NB SET; the length of the scale bar is 5 μm; (c) output characteristics of the ZnO NB SET at room temperature; (d) transfer characteristics at room temperature indicating n-type conductivity in the NB.

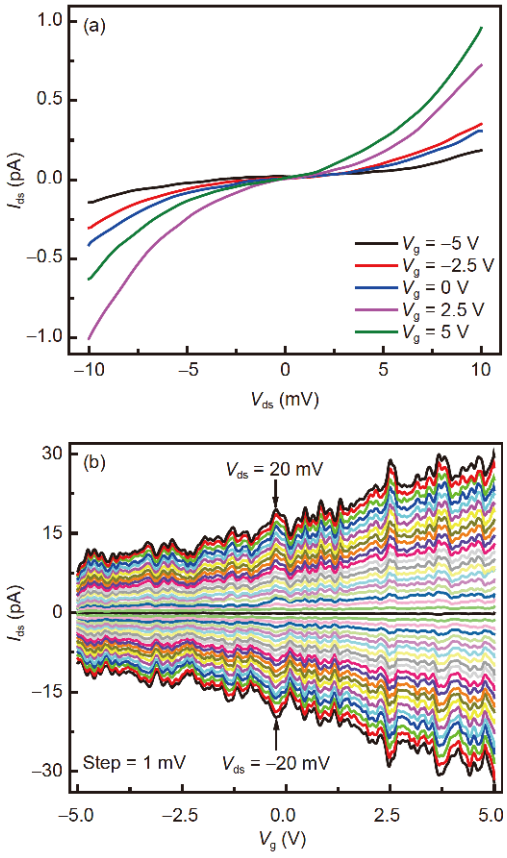

Figure 2 (Color online) (a) Output characteristics of the ZnO NB SET at 4.2 K; the non-monotonic increase current shows the presence of the Coulomb blockade effect; (b) transfer characteristic curves of the SET at 4.2 K show clear Coulomb oscillations.

multiple tunnel junctions theory [54]. The uneven distribution of component and structure in ZnO provides random potentials, forming the in-plane (x and y) two-dimensional confinement. The thickness of the ZnO NB provides another confinement along the z direction. These three-dimensional confinements constitute quantum dots in the ZnO NB, as has been demonstrated in previous work [6,26]. These dots are similar to the quantum dots in Si nanowires, in which the Si quantum dots and the tunnel barriers are self-formed by a volumetric undulation process [55]. The period of oscillations in Figure 3(a) is approximately 0.25 V, whereas the average period of oscillations in Figure 3(b) is 0.18 V. The asymmetry of oscillations for positive and negative source-drain bias can be ascribed to the non-uniform distribution of quantum dots in the ZnO NB. Because of random distribution, the tunneling barrier between the metal electrodes and quantum dots cannot be exactly the same [5].

The contour plots for differential trans-conductance as a function of gate voltage are shown in Figure 3(c) and (d), in which the gate voltage range is the same as that shown in Figure 3(a) and (b). The black dotted lines in the figures show the Coulomb diamonds. Figure 3(c) shows uniform Coulomb diamonds, whereas Coulomb diamonds of different sizes are observed in Figure 3(d). The regions above the Coulomb diamonds correspond to the higher values of the trans-conductance. The island-gate capacitance C_g of the SET can be calculated as follows [24,46]:

$$C_g = e / \Delta V_g, \tag{1}$$

where ΔV_g is the period of oscillation and e is the electronic

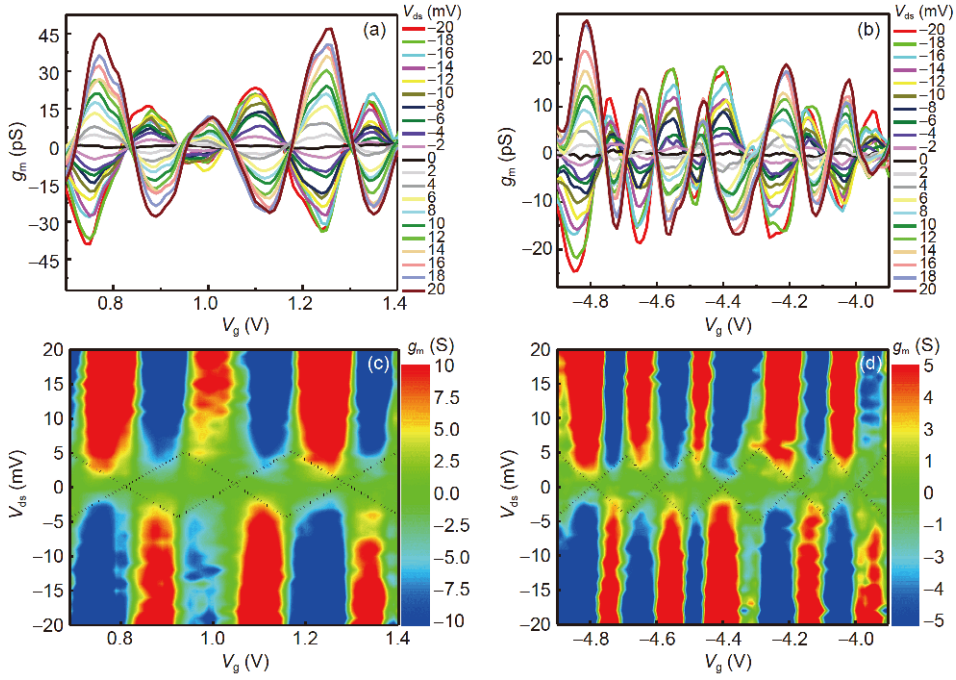

Figure 3 (Color online) Conductance oscillations in the ZnO NB SET at 4.2 K. (a) With uniform Coulomb gap; (b) with non-uniform Coulomb gap; contour plots of differential trans-conductance at 4.2 K; (c) for single-tunneling quantum dots; (d) for multi-tunneling junctions.

charge. The island-gate capacitance in the case of single and multi-quantum dots is 0.64 and 0.88 aF, respectively. By extrapolating the edge of the Coulomb diamond, the total capacitance C_t of the SET can be found using the expression [24]

$$C_t = e / V_b, \quad (2)$$

where V_b is the bias voltage at the Coulomb diamond edge. The total capacitance for the single and multi-quantum dots system is 40 and 32 aF, respectively. The charging energy E_c required for electrons to tunnel to the quantum dot can be estimated by the expression [24,46,56]

$$E_c = e^2 / C_t, \quad (3)$$

where C_t is the total capacitance calculated using eq. (2). The charging energy is 4 meV and approximately 5 meV in the case of the single and multi-quantum dots system, respectively. If we assume the shape of the quantum dot to be spherical, then its radius can be calculated by [39]

$$C_t = 4\pi\varepsilon_r\varepsilon_o r, \quad (4)$$

where ε_o is the permittivity of the free space, ε_r is the dielectric constant of ZnO, and r is the radius of the quantum dot. The diameter of the single quantum dot was calculated to be 86 nm, whereas the average diameter in the case of the multi-dot system was in the range of 70 nm, with a dielectric constant of ZnO of 8.2 [5,6]. Here, we assume the quantum dot to be spherical just to give a rough idea of the size of the dots. The charging energy obtained in our ZnO single quantum dot at low temperature is comparable with that in previous reports on single nanowire SETs [26,46]. In principle, if the size of the quantum dot can be reduced further during fabrication through lithographic techniques, single-electron charging effects in ZnO NBs can also be observed at room temperature, as in the case of other materials [25,57,58].

In single-electron pumping, an AC signal is applied, which periodically perturbs the system and produces a quantized DC current [41,59,60]. Mostly isolated quantum dot configuration for the charge pumping is used. If the quantum dot in a SET is pumped with an AC signal of frequency f, then the quantized current $I = nef$ is produced, where n is the number of pumped electrons [29,31,61]. For single-electron pumping in ZnO NB transistors with quantum dots, which is distributed into the NB and separated by tunnel junctions between source and drain electrodes, we used a simple configuration without the presence of any additional top or side gates to control the height of the tunnel barrier. The charging energy levels within the quantum dot and tunnel barrier between source electrode and quantum dots can be modulated by applying an AC signal to the back-gate, which has capacitive coupling with the quantum dot. Normally, single-electron pumping consists of four processes, namely: (i) loading the electron to the quantum dot; (ii) electron back-tunneling from the quantum dot; (iii) trapping the electron in the quantum dot; (iv) ejection of the electron from the quantum dot [51,62]. The mechanism can be explained with the help of a schematic of the applied AC signal and its effect on the tunnel barrier, as shown in Figure 4. By applying positive AC voltage to the gate electrode, the barrier between source terminal and quantum dot is lowered and some of the electrons from the source terminal are loaded into the island, as shown in Figure 4(a(i)). As the gate bias decreases, the barrier between quantum dot and source terminal increases and the loaded electrons then align themselves in different discrete energy levels in the quantum dot. The electron with higher-energy tunnels back to the source terminal, as shown in Figure 4(a(ii)). The probability of the back-tunneling of the lower-energy electron is many orders of magnitude less than the higher-energy electron. Upon further decrease in gate bias, the electron in the quantum dot is trapped because of the increased barrier, as depicted in Figure 4(a(iii)). As the gate bias further reduces, the tunnel barrier height increases and the electron escapes from the quantum dot to the drain terminal, as presented in Figure 4(a(iv)). Figure 4(b) indicates the shape of the pulse applied for single-electron pumping, indicating the different steps of the pumping mechanism at corresponding values.

Single- and double-electron pumping in the ZnO quantum dot was successfully achieved by applying an AC signal of pulse wave. The single-electron pumping in the ZnO quantum dot is shown as the bottom curve in Figure 5(a). The values of bias voltage and pump voltage used were 5 mV and 3 V, respectively. The frequency of AC signal varied from 1 to 25 MHz. The current under the applied frequency signal

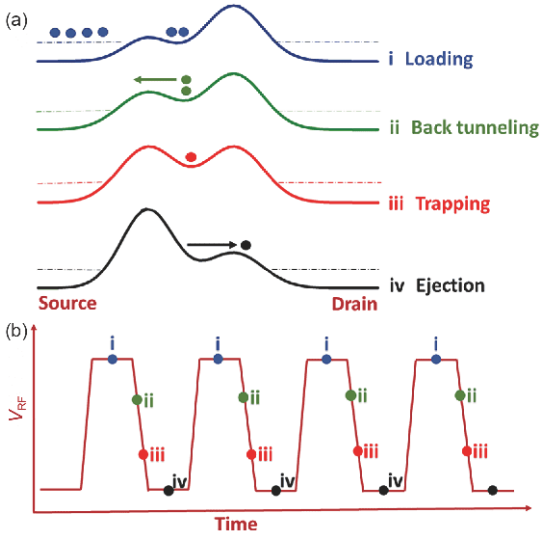

Figure 4 (Color online) (a) Schematic diagram of pumping mechanism in ZnO quantum dot, indicating four phases during the pump cycle: (i) loading electron in quantum dot; (ii) electron back-tunneling from quantum dot; (iii) trapping electron in quantum dot; and (iv) ejection of electron from quantum dot. (b) Pulse waveform applied to the back-gate for pumping electrons, with labeling of different stages.

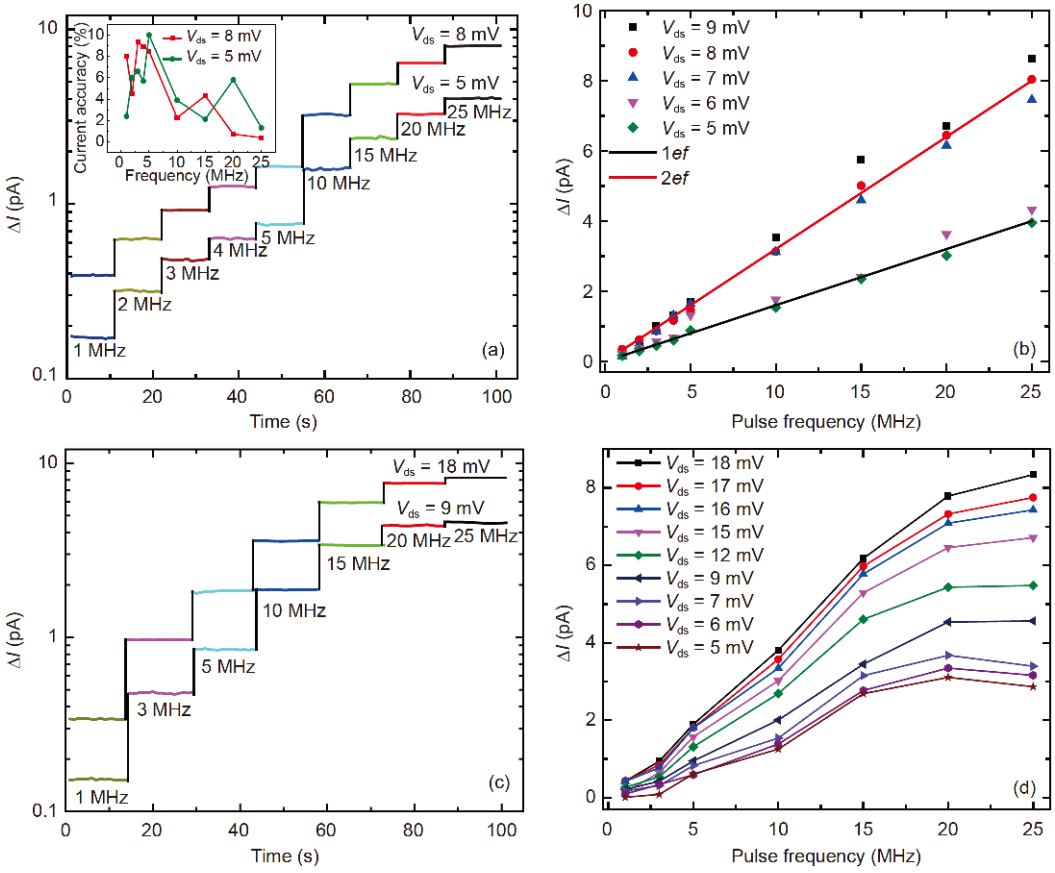

Figure 5 (Color online) Single- and double-electron pumping in ZnO quantum dot. (a) Pump voltage of 3 V with source bias voltages at 5 and 8 mV; (c) pump voltage of 2.7 V and source bias of 9 and 18 mV, respectively. The horizontal axis (time) is used for the representation; the current does not depend on time. The inset shows the accuracy in the pumping current with applied frequency for single- and double-electron pumping. Pumping current as a function of pulse frequency for various bias voltage: for pump voltages of (b) 3 and (d) 2.7 V. In (b), the solid straight lines show the calculated current values, whereas the dots show the experimental value of the current for corresponding frequencies.

does not depend on the horizontal axis parameter (time). It is just the representation of the change in current with that in the applied frequency. Clear quantized current levels for all frequency values were achieved, showing the discrete number of pumped electrons. Double-electron pumping was also achieved by simply changing the bias voltage from 5 to 8 mV, which is shown as the top curve in Figure 5(a).

To see the clear effect of the frequency of the applied signal on the pumping current, pumping current against signal frequency has been plotted and is shown in Figure 5(b). The solid lines represent the calculated values of the current for single and double electrons at particular frequencies, whereas the dots show the experimental results. The pumping current increases linearly with the applied signal frequency, satisfying the relation $\Delta I=nef$, where n represents the number of electrons. When V_{ds} increased from 5 to 6 meV, only one single-electron pumping appeared in ZnO, as indicated by the black solid line in Figure 5(b), whereas for V_{ds} from 7 to 9 meV, double-electron pumping occurs and the pumping current is equal to $2ef$, as shown by the red line in Figure 5(b). The effect of source bias voltage on the pumping current was also observed. The pumping current increases in a discrete manner for a particular range of the source bias, indicating the pumping through a single island. The accuracy in the pumping current with applied frequency is shown as an inset in Figure 5(a). The accuracy was calculated by the relative change in reference (calculated) values and the mean precise value of the pumping current. The accuracy decreases from 8% to 1% when the frequency increases from 1 to 25 MHz at both applied bias for single- and double-electron pumping. This is due to the relatively large background current noise at low frequency range during the measurement, which is rather small at high frequency. Accuracy can be further improved by fabricating single quantum dot SETs using lithographic techniques in the future and by suppressing the background current noise level.

The pump voltage also affects the pumping current. We observed single- and double-electron pumping for different values of pump voltage. The value of pump voltage used in this case was 2.7 V, and the frequency varied from 1 to 25 MHz. This value of pump voltage was lower than that used for the case discussed in Figure 5(a), where a pump voltage of 3 V was used. However, in this case, higher values of V_{ds} (9 and 18 mV) were required to overcome the tun-

neling barrier between the quantum dot and source electrode in comparison with the case discussed in Figure 5(a), where the V_{ds} values were 5 and 8 mV, respectively. Figure 5(c) shows single-electron pumping at a source bias of 9 mV (bottom curve). Here, the current level for single-electron pumping was achieved for the applied frequency of up to 20 MHz. With a further increase in frequency of the signal, the electron pumping is no more discrete, and saturation of the current arises. By increasing the bias voltage, double-electron pumping was also observed in the ZnO quantum dot with an applied frequency of up to 20 MHz, shown as the top curve in Figure 5(c), and saturation in the current occurs at higher frequencies. Signal frequency-dependent pumping current is also shown in Figure 5(d). This saturation of pumping current at higher frequencies can be attributed to fractional electron tunneling rather than discrete electron tunneling during each cycle of the applied signal [60]. This controlled quantized single- and double-electron pumping in the ZnO quantum dot is advantageous in its precise control of electron injection and detection.

So far, single-electron pumping in InAs nanowire single and double quantum dots in different device configurations has been observed by using a combination of global back-gate and local bottom gates and by applying a periodic pulse sequence to two plunger gates, respectively [63,64]. Additionally, single-electron pumping has been demonstrated numerically and experimentally in phosphorus-doped Si nanowire multi-tunneling junctions formed by the discrete distribution of phosphorus in the nanowire at 5.5 K [65]. In comparison with previous reports, single-electron pumping in ZnO quantum dots is demonstrated in one and two electron levels only by universal back-gate, which eliminates the complexities of device fabrication. The realization of electron pumping in ZnO quantum dots at low temperature is promising. However, for room temperature devices, the Coulomb charging energy in SETs needs to exceed thermal energy (k_BT), which can be achieved by designing devices with a small island size using microfabrication techniques [66,67]. Therefore, from the application point of view, a ZnO NB-based device can be optimized to operate at room temperature by fabricating quantum dots with specified designs, especially of a smaller size with precision confinement as desired.

4 Conclusions

In conclusion, we fabricated ZnO NB SETs. Strong Coulomb oscillations were observed at 4.2 K. The periodic and non-periodic Coulomb diamonds observed were attributed to the presence of single uniform quantum dots and multi-quantum dots, respectively. The charging energy values were 4 and 5 meV in the case of the single and multi-dots systems, respectively, and the corresponding diameters of the quantum dots were approximately 86 and 70 nm. Single-electron quantum dot pumping was also achieved by applying back-gated AC signals with varying frequencies. Double-electron pumping was also realized by varying the source-drain bias and pump voltage. A 1% accuracy in the current in single- and double-electron pumping was achieved at high frequencies. Discrete and continuous increases in the pump current against the signal frequency applied were achieved by varying the source bias voltage at different pump voltages. Saturation of the pumping current according to frequency was attributed to fractional tunneling of the electrons rather than discrete tunneling. Precise controlled single- and double-electron pumping can be employed in many quantum computing and metrological applications.

This work was supported by the National Natural Science Foundation of China (Grant Nos. 51761145104, 11934019, 61675228, 11721404, and 11874419), the Strategic Priority Research Program, the Instrument Developing Project and the Interdisciplinary Innovation Team of the Chinese Academy of Sciences (Grant Nos. XDB28000000, and YJKYYQ20180036), and the Key R & D Program of Guangdong Province (Grant No. 2018B030329001).

1 T. Dietl, Nat. Mater. **9**, 965 (2010).
2 T. Dietl, H. Ohno, F. Matsukura, J. Cibert, and D. Ferrand, Science **287**, 1019 (2000).
3 J. Tang, C. Y. Wang, L. T. Chang, Y. Fan, T. Nie, M. Chan, W. Jiang, Y. T. Chen, H. J. Yang, H. Y. Tuan, L. J. Chen, and K. L. Wang, Nano Lett. **13**, 4036 (2013).
4 Y. Ohno, D. K. Young, B. Beschoten, F. Matsukura, H. Ohno, and D. D. Awschalom, Nature **402**, 790 (1999).
5 X. Xu, A. C. Irvine, Y. Yang, X. Zhang, and D. A. Williams, Phys. Rev. B **82**, 195309 (2010).
6 X. F. Ji, Z. Xu, S. Cao, K. S. Qiu, J. Tang, X. T. Zhang, and X. L. Xu, Chin. Phys. Lett. **31**, 067303 (2014).
7 R. Araneo, F. Bini, A. Rinaldi, A. Notargiacomo, M. Pea, and S. Celozzi, Nanotechnology **26**, 265402 (2015).
8 Z. L. Wang, and J. Song, Science **312**, 242 (2006).
9 Z. Li, X. Zhang, and G. Li, Phys. Chem. Chem. Phys. **16**, 5475 (2014).
10 Y. Hu, Y. Chang, P. Fei, R. L. Snyder, and Z. L. Wang, ACS Nano **4**, 1234 (2010).
11 J. Bao, M. A. Zimmler, F. Capasso, X. Wang, and Z. F. Ren, Nano Lett. **6**, 1719 (2006).
12 Z. Dai, A. Nurbawono, A. Zhang, M. Zhou, Y. P. Feng, G. W. Ho, and C. Zhang, J. Chem. Phys. **134**, 104706 (2011).
13 J. Song, J. Zhou, and Z. L. Wang, Nano Lett. **6**, 1656 (2006).
14 N. Janssen, K. M. Whitaker, D. R. Gamelin, and R. Bratschitsch, Nano Lett. **8**, 1991 (2008).
15 V. Modepalli, M. J. Jin, J. Park, J. Jo, J. H. Kim, J. M. Baik, C. Seo, J. Kim, and J. W. Yoo, ACS Nano **10**, 4618 (2016).
16 A. Singhal, S. N. Achary, J. Manjanna, S. Chatterjee, P. Ayyub, and A. K. Tyagi, J. Phys. Chem. C **114**, 3422 (2010).
17 M. A. Laakso, T. Ojanen, and T. T. Heikkilä, Phys. Rev. B **77**, 233303 (2008).
18 S. Kano, Y. Azuma, K. Maeda, D. Tanaka, M. Sakamoto, T. Teranishi, L. W. Smith, C. G. Smith, and Y. Majima, ACS Nano **6**, 9972 (2012).
19 M. A. Laakso, T. T. Heikkilä, and Y. V. Nazarov, Phys. Rev. Lett. **104**, 196805 (2010).
20 M. H. Devoret, and R. J. Schoelkopf, Nature **406**, 1039 (2000).
21 Z. B. Tan, G. T. Liu, L. Lu, and C. L. Yang, Sci. China-Phys. Mech. Astron. **55**, 7 (2012).

22 Z. Bai, X. Liu, Z. Lian, K. Zhang, G. Wang, S. F. Shi, X. Pi, and F. Song, Chin. Phys. Lett. **35**, 037301 (2018).
23 M. Turek, J. Siewert, and K. Richter, Phys. Rev. B **71**, 220503 (2005).
24 Y. T. Tan, T. Kamiya, Z. A. K. Durrani, and H. Ahmed, J. Appl. Phys. **94**, 633 (2003).
25 M. T. Björk, C. Thelander, A. E. Hansen, L. E. Jensen, M. W. Larsson, L. R. Wallenberg, and L. Samuelson, Nano Lett. **4**, 1621 (2004).
26 J. P. Pekola, K. P. Hirvi, J. P. Kauppinen, and M. A. Paalanen, Phys. Rev. Lett. **73**, 2903 (1994).
27 M. D. LaHaye, O. Buu, B. Camarota, and K. C. Schwab, Science **304**, 74 (2004).
28 X. Xu, H. Baker, and D. A. Williams, Nano Lett. **10**, 1364 (2010).
29 P. J. Leek, M. R. Buitelaar, V. I. Talyanskii, C. G. Smith, D. Anderson, G. A. C. Jones, J. Wei, and D. H. Cobden, Phys. Rev. Lett. **95**, 256802 (2005).
30 L. J. Geerligs, V. F. Anderegg, P. A. M. Holweg, J. E. Mooij, H. Pothier, D. Esteve, C. Urbina, and M. H. Devoret, Phys. Rev. Lett. **64**, 2691 (1990).
31 X. Jehl, B. Voisin, T. Charron, P. Clapera, S. Ray, B. Roche, M. Sanquer, S. Djordjevic, L. Devoille, R. Wacquez, and M. Vinet, Phys. Rev. X **3**, 021012 (2013).
32 L. Fricke, M. Wulf, B. Kaestner, F. Hohls, P. Mirovsky, B. Mackrodt, R. Dolata, T. Weimann, K. Pierz, U. Siegner, and H. W. Schumacher, Phys. Rev. Lett. **112**, 226803 (2014).
33 B. Kaestner, V. Kashcheyevs, G. Hein, K. Pierz, U. Siegner, and H. Schumacher, Appl. Phys. Lett. **92**, 192106 (2008).
34 M. R. Connolly, K. L. Chiu, S. P. Giblin, M. Kataoka, J. D. Fletcher, C. Chua, J. P. Griffiths, G. A. C. Jones, V. I. Fal'ko, C. G. Smith, and T. J. B. M. Janssen, Nat. Nanotech. **8**, 417 (2013).
35 W. Y. Fu, L. Liu, W. L. Wang, M. H. Wu, Z. Xu, X. D. Bai, and E. G. Wang, Sci. China-Phys. Mech. Astron. **53**, 828 (2010).
36 X. Q. Zhang, X. W. Xia, J. P. Xu, M. T. Cheng, and Y. P. Yang, Chin. Phys. B **28**, 114207 (2019).
37 H. Pothier, P. Lafarge, C. Urbina, D. Esteve, and M. H. Devoret, Europhys. Lett. **17**, 249 (1992).
38 F. Kuemmeth, K. I. Bolotin, S. F. Shi, and D. C. Ralph, Nano Lett. **8**, 4506 (2008).
39 M. Manoharan, Y. Tsuchiya, S. Oda, and H. Mizuta, Nano Lett. **8**, 4648 (2008).
40 K. Ohkura, T. Kitade, and A. Nakajima, J. Appl. Phys. **98**, 124503 (2005).
41 G. Yamahata, S. P. Giblin, M. Kataoka, T. Karasawa, and A. Fujiwara, Appl. Phys. Lett. **109**, 013101 (2016).
42 L. P. Kouwenhoven, A. T. Johnson, N. C. van der Vaart, C. J. P. M. Harmans, and C. T. Foxon, Phys. Rev. Lett. **67**, 1626 (1991).
43 J. M. Elzerman, R. Hanson, J. S. Greidanus, L. H. Willems van Beveren, S. De Franceschi, L. M. K. Vandersypen, S. Tarucha, and L. P. Kouwenhoven, Phys. Rev. B **67**, 161308 (2003).
44 L. X. Zhang, P. Matagne, J. P. Leburton, R. Hanson, and L. P. Kouwenhoven, Phys. Rev. B **69**, 245301 (2004).
45 H. A. Nilsson, T. Duty, S. Abay, C. Wilson, J. B. Wagner, C. Thelander, P. Delsing, and L. Samuelson, Nano Lett. **8**, 872 (2008).
46 C. Thelander, T. Mårtensson, M. T. Björk, B. J. Ohlsson, M. W. Larsson, L. R. Wallenberg, and L. Samuelson, Appl. Phys. Lett. **83**, 2052 (2003).
47 M. P. van Kouwen, M. E. Reimer, A. W. Hidma, M. H. M. van Weert, R. E. Algra, E. P. A. M. Bakkers, L. P. Kouwenhoven, and V. Zwiller, Nano Lett. **10**, 1817 (2010).
48 J. Wunderlich, T. Jungwirth, B. Kaestner, A. C. Irvine, A. B. Shick, N. Stone, K. Y. Wang, U. Rana, A. D. Giddings, C. T. Foxon, R. P. Campion, D. A. Williams, and B. L. Gallagher, Phys. Rev. Lett. **97**, 077201 (2006).
49 L. Wu, X. T. Zhang, Z. Wang, Y. Liang, and H. Xu, J. Phys. D-Appl. Phys. **41**, 195406 (2008).
50 X. Zhang, H. Lu, H. Gao, X. Wang, H. Xu, Q. Li, and S. Hark, Crystal Growth Design **9**, 364 (2008).
51 B. A. Turek, K. W. Lehnert, A. Clerk, D. Gunnarsson, K. Bladh, P. Delsing, and R. J. Schoelkopf, Phys. Rev. B **71**, 193304 (2005).
52 I. Bâldea, and H. Köppel, Phys. Rev. B **79**, 165317 (2009).
53 M. H. Devoret, D. Esteve, and C. Urbina, Nature **360**, 547 (1992).
54 H. Grabert, Zeitschrift Phys. B Condens. Matter **85**, 319 (1991).
55 S. Lee, Y. Lee, E. B. Song, and T. Hiramoto, Nano Lett. **14**, 71 (2014).
56 K. Aravind, Y. W. Su, I. L. Ho, C. S. Wu, K. S. Chang-Liao, W. F. Su, K. H. Chen, L. C. Chen, and C. D. Chen, Appl. Phys. Lett. **95**, 092110 (2009).
57 M. A. Rafiq, K. Masubuchi, Z. A. Durrani, A. Colli, H. Mizuta, W. I. Milne, and Oda S, Jpn J. Appl. Phys. **51**, 025202 (2012).
58 Z. A. K. Durrani, and M. A. Rafiq, MicroElectron. Eng. **86**, 456 (2009).
59 P. Devillard, V. Gasparian, and T. Martin, Phys. Rev. B **78**, 085130 (2008).
60 C. Y. Lin, and W. M. Zhang, Appl. Phys. Lett. **99**, 072105 (2011).
61 J. van der Heijden, G. Tettamanzi, and S. Rogge, Sci. Rep. **7**, 44371 (2017).
62 S. Giblin, M. Kataoka, J. Fletcher, P. See, T. Janssen, J. Griffiths, G. Jones, I. Farrer, and D. Ritchie, arXiv: 1201.2533.
63 A. Fuhrer, C. Fasth, and L. Samuelson, Appl. Phys. Lett. **91**, 052109 (2007).
64 S. d'Hollosy, M. Jung, A. Baumgartner, V. A. Guzenko, M. H. Madsen, J. Nygård, and C. Schönenberger, Nano Lett. **15**, 4585 (2015).
65 D. Moraru, Y. Ono, H. Inokawa, and M. Tabe, Phys. Rev. B **76**, 075332 (2007).
66 H. W. Postma, T. Teepen, Z. Yao, M. Grifoni, and C. Dekker, Science **293**, 76 (2001).
67 D. Zahid Ali Khan, *Single-Electron Devices and Circuits in Silicon* (World Scientific, Singapore, 2010).